Spin Injection, Manipulation, and Detection in Semiconductors

by

Ayomipo I. Ojo

A report submitted for the credentials check

Department of Physics

College of Arts and Sciences

University of South Florida

Major Professor: Darío A. Arena, Ph.D.

Co-Major Professor: Manh-Huong Phan, Ph.D.

Inna Ponomareva, Ph.D.

August 2024

CONTENTS

I. INTRODUCTION

Traditional semiconductor devices rely on the manipulation of charge to store and transmit information. However, increasing power consumption and heat generation are becoming significant concerns in the semiconductor industry, limiting the operating speeds of semiconductor chips. Additionally, further miniaturization of these chips faces considerable challenges. Consequently, there is a pressing need to find better alternatives that can either complement or replace the existing technology. Spintronics offers a novel approach by incorporating the electron's spin, alongside its charge, into device functionality. This paradigm shift provides several advantages over traditional charge-based semiconductor devices, including increased data storage density, non-volatility, lower power consumption, and higher operational speeds.

In some semiconductors like GaAs, spin-orbit coupling causes the valence band to split into two subbands: an upper subband ($j = 3/2$) and a lower subband ($j = 1/2$). The upper valence subband is further divided into a light hole subband ($|m_j| = 1/2$) and a heavy hole subband ($|m_j| = 3/2$), as illustrated in Fig. 1a. In 1968, Lampel [1] demonstrated the possibility of creating a non-equilibrium spin distribution of electrons in Si by illuminating it with circularly polarized light. When the photon energy, E, lies within the range $E_g \leq E < E_g + \Delta$, where E_g is the bandgap and Δ is the splitting between the upper and lower valence subband, transitions from the heavy hole and light hole subbands to the conduction band can be induced. These transitions are governed by optical transition selection rules based on the helicity of the circularly polarized light, a process known as optical spin orientation. However, this process is inefficient in an indirect bandgap semiconductor like Si due to the spin relaxation time being much shorter than the carrier recombination time [2]. Consequently, research efforts shifted towards direct bandgap semiconductors such as GaAs, which are more favorable to efficient optical spin orientation.

The fundamental concept of a spin transistor was introduced by Datta and Das [3]. By considering the zero-field spin splitting and spin precession occurring in a two-dimensional electron gas (2DEG) due to the dominant Rashba term in the Hamiltonian that arises from the perpendicular electric field at the heterojunction interface, they proposed a device analogous to the electro-optic light modulator. This device employs magnetic contacts to preferentially inject and detect spin orientation in narrow-gap semiconductors such as InGaAs (Fig. 1b). Building upon their pioneering work, several spin-based devices, including spin light-emitting diodes (LED) [4], all-spin logic [5], and spin-based field programmable gate arrays [6] have been proposed.

This review provides an overview of the significant advancements and persistent challenges in
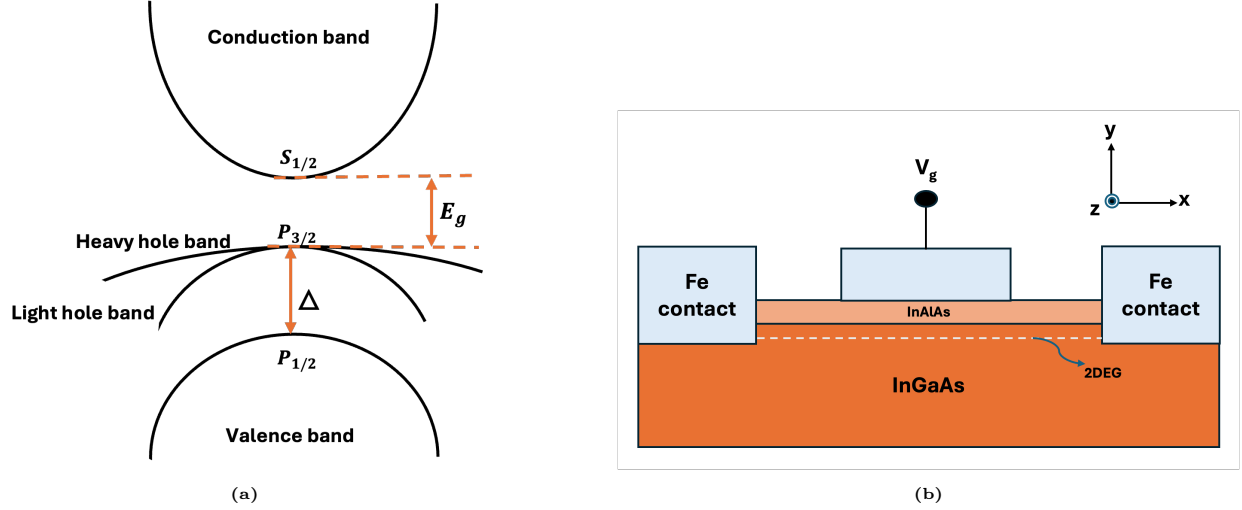
3

FIG. 1: (a) Valence band-splitting in a direct bandgap semiconductor due to spin-orbit coupling (b) Concept of a spin-transistor.

the electrical injection, manipulation, and detection of spins in semiconductors.

II. ELECTRICAL SPIN INJECTION

A. Fundamental problem: conductivity mismatch

A major factor affecting efficient electrical spin injection from a ferromagnetic material to a semiconductor is the conductivity mismatch between the two materials [7]. Assuming we are in the linear response regime where the conductivity of the system remains the same throughout the experiment and all excitation energies are less than $k_B T$, the electrochemical potential is different for spin-down and spin-up electrons. Ohm's law for both spin channels is given as [8]

$$\vec{\nabla}\mu^{\uparrow\downarrow} = -\left(\frac{e\vec{j}^{\uparrow\downarrow}}{\sigma^{\uparrow\downarrow}}\right) \tag{1}$$

where $\sigma^{\uparrow\downarrow}$ represents the conductivities for the spin-up and spin-down channels respectively, $j^{\uparrow\downarrow}$ are the current densities for the respective spin directions, and e is the electron charge. In spin-polarized transport, the total current density must be continuous at the interface i.e. $\nabla(j^{\uparrow} + j^{\downarrow}) = 0$. The interaction between the two spin channels can be described by the following diffusion equation [8]:

$$\frac{\mu^{\uparrow} - \mu^{\downarrow}}{\tau_s} = D\nabla(\mu^{\uparrow} - \mu^{\downarrow}) \tag{2}$$

4

where τ_s is the spin-flip time, $\mu^\uparrow(\mu^\downarrow)$ is the electrochemical potential for spin-up (spin-down) channel, and D is the weighted diffusion constant. To solve equation 2, the boundary conditions are based on the assumptions that $\mu^{\uparrow\downarrow}$ is continuous at any interface and $\mu^\uparrow$ and $\mu^\downarrow$ are equal at $\pm\infty$. In a ferromagnet, $\mu^\uparrow$ and $\mu^\downarrow$ are different. Any current passing through the ferromagnet/semiconductor interface causes a splitting of the electrochemical potentials (spin accumulation) for the two spin directions. This spin accumulation decays away from the interface over a distance characterized by the spin-flip length $\lambda = \sqrt{D\tau_s}$ [9] as shown in Fig. 2a. The FM/SC device can be modeled using a two-current resistor model assuming that the length scales being probed are comparable to the spin-flip length. This is crucial because additional spin flips within the device diminish the usable spin polarization [8].

In the parallel circuit (Fig. 2b), the resistances for the different spin channels in the FM are given by [9]

$$R_{fm}^{\uparrow\downarrow} = \frac{2R_{fm}}{1 \pm \beta} \tag{3}$$

where R_{fm} is the total resistance of the FM and $\beta = \dfrac{\sigma^\uparrow - \sigma^\downarrow}{\sigma^\uparrow + \sigma^\downarrow}$ is the bulk spin polarization in the FM. Also, in the spin-unpolarized semiconductor, the resistance of each spin channel is $2R_{sc}$. The current spin polarization, α is given by [9]

$$\alpha = \beta \frac{R_{fm}}{R_{sc}} \left(\frac{1}{\dfrac{R_{fm}}{R_{sc}} + (1 - \beta^2)} \right) \tag{4}$$

Restricting the analysis to the spin flip length scale, R_{fm} and R_{sc} can be replaced by $\frac{\lambda_{fm}}{\sigma_{fm}}$ and $\frac{\lambda_{sc}}{\sigma_{sc}}$ respectively. Hence, α is given by [9]:

$$\alpha = \beta \frac{\lambda_{fm}}{\lambda_{sc}} \frac{\sigma_{sc}}{\sigma_{fm}} \left(\frac{1}{\dfrac{\lambda_{fm}}{\lambda_{sc}} \dfrac{\sigma_{sc}}{\sigma_{fm}} + (1 - \beta^2)} \right) \tag{5}$$

It is clear that the current spin polarization is proportional to the bulk spin polarization in the FM and the ratio $\frac{\sigma_{sc}}{\sigma_{fm}}$. In principle, $\frac{\sigma_{sc}}{\sigma_{fm}}$ is very small hence this conductivity mismatch gives rise to a negligible current spin polarization and consequently inefficient spin injection.
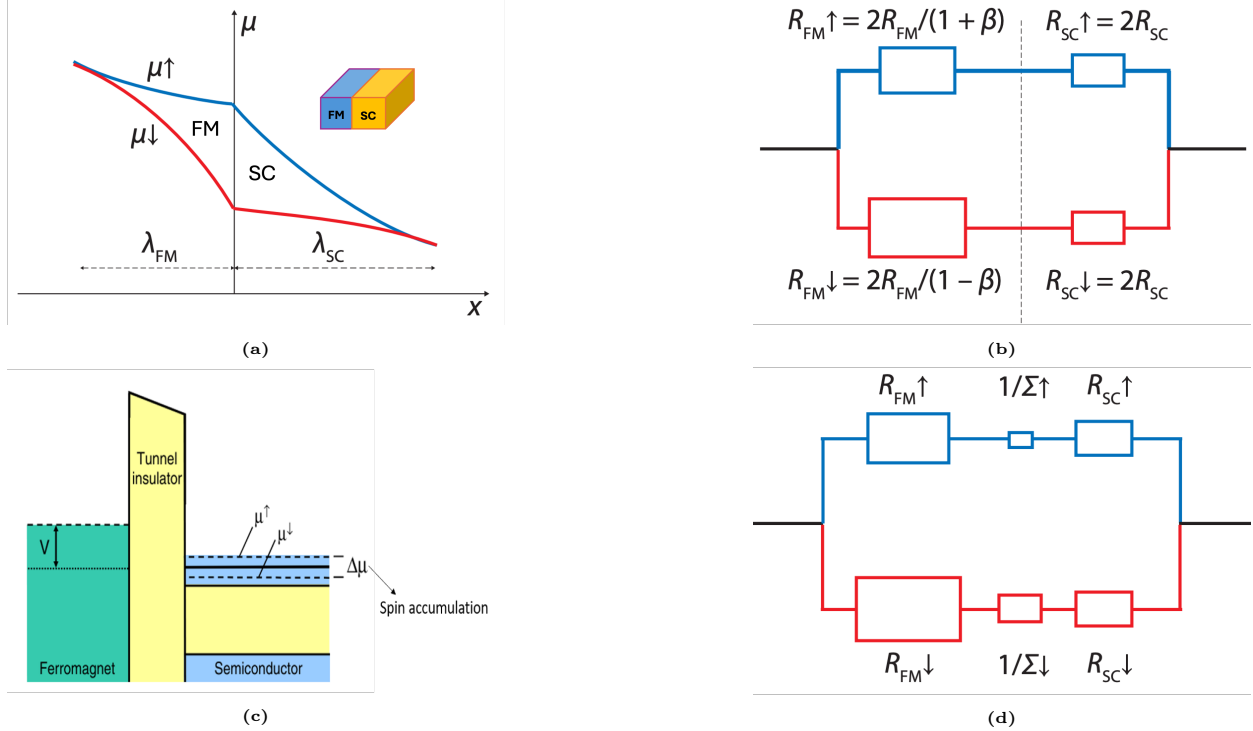
FIG. 2: (a) Splitting of the electrochemical potential at the FM/SC interface as current flows. Inset shows the FM/SC device [9] (b) Two-current resistor model for the FM/SC device [9] (c) Schematic illustration of an FM/insulator(T)/SC tunnel junction [10] (d) Two-current resistor model for the FM/T/SC device [9].

B. Possible solutions to the conductivity mismatch

1. Spin-polarized injectors

The use of ferromagnetic semiconductors has been explored as a promising approach to overcome the conductivity mismatch between metals and semiconductors. Fiederling *et al.* [4] demonstrated the effectiveness of $Be_xMn_yZn_{1-x-y}Se$ as a spin aligner, achieving a 90% spin injection efficiency by injecting spin-polarized electrons into a GaAs/AlGaAs LED. Ohno and co-workers [11] used a $Ga_xMn_{1-x}As$ ferromagnetic p-type semiconductor and the n-type GaAs substrate to inject spin-polarized holes and unpolarized electrons under forward bias into (In,Ga)As quantum well (QW) respectively. Despite these significant achievements, the Curie temperature of magnetic semiconductors remains below room temperature, thus limiting their integration into conventional technologies.

Half-metallic materials are considered ideal spin injectors because of their exceptionally high spin polarization and Curie temperatures that exceed room temperature. In a half-metal, the Fermi level is uniquely positioned to exhibit metallic behavior for one spin orientation, where it intersects a partially filled electronic band, allowing for conduction. For the opposite spin orientation, the Fermi

6

level lies within a band gap, resulting in insulating or semiconducting behavior with no available electronic states. This unique electronic structure results in fully spin-polarized carriers at the Fermi level [12]. Heusler alloys, particularly Co_2YZ (Y= Fe or Mn, Z= Si, Ge, Ga, Al) compounds have been reported to show half-metallic properties in the fully ordered $L2_1$ phase [13, 14]. Despite the theoretically predicted 100% spin polarization in half-metallic Heusler alloys, experimental results have demonstrated significantly lower values. This reduced spin polarization has been attributed to factors such as atomic disorder, the in-diffusion of magnetic impurities into the semiconductor due to the high temperatures used during the growth process, and interfacial reactions [15–17]. In 2005, successful electrical spin injection from Co_2MnGe into an $Al_{0.1}Ga_{0.9}As/GaAs$ heterostructure was demonstrated at 2 K, achieving $\sim 27\%$ spin polarization [18]. Subsequently, Ramsteiner *et al.* [16] reported a spin injection efficiency of at least 50% at 20 K using Co_2FeSi as a spin injector in a GaAs spin-LED. Furthermore, at 5K, Damsgaard and co-workers [19] measured a 6.4% spin polarization with an epitaxial Co_2MnGa spin injector deposited on GaAs (001).

2. Tunnel barriers

To circumvent the conductance mismatch, Rashba [20] showed that a spin-selective tunnel contact in the FM/SC interface decreases the conductivity mismatch thereby increasing spin injection efficiency. The spin injection results in an imbalance of polarized electrons in the semiconductors which can be described by a spin splitting $\Delta\mu = \mu^\uparrow - \mu^\downarrow$ of the electrochemical potential as shown in Fig. 2c. An ideal tunnel barrier must exhibit uniform thickness to ensure consistent tunneling probability, minimal defects to prevent scattering and maintain spin coherence, and a low resistance-area product to reduce power consumption and allow efficient operation at lower voltages [21]. Additionally, it should be highly compatible with both the ferromagnetic material and the semiconductor to form stable, high-quality interfaces that preserve spin polarization and prevent the formation of interfacial states or Schottky barriers, ensuring efficient spin transfer and retention across the interface. Taniyama *et. al* [9] have shown that the current spin polarization in this FM/T/SC device can be obtained as

$$\alpha = \beta \frac{r_{fm}}{r_{fm} + r_{sc} + r_c} + \frac{1/\Sigma^\downarrow - 1/\Sigma^\uparrow}{1/\Sigma^\downarrow + 1/\Sigma^\uparrow} \frac{r_c}{r_{fm} + r_{sc} + r_c} \tag{6}$$

where $\Sigma_{\uparrow\downarrow}$ are the tunnel contact conductances for the different spin channels. Since the contact resistance $r_c \gg r_{fm}, r_{sc}$, equation 6 reduces to $\alpha \approx \dfrac{\Sigma^\uparrow - \Sigma^\downarrow}{\Sigma^\downarrow + \Sigma^\uparrow}$. This implies that the electrical
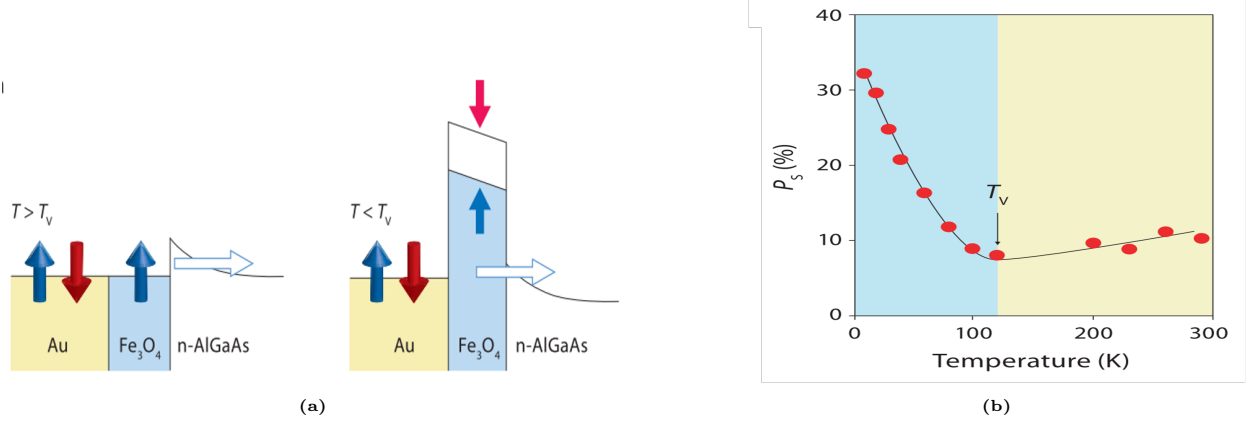
FIG. 3: (a) Spin injection mechanism through an Fe_3O_4 layer, both above and below T_V (b) Spin polarization as a function of temperature across T_V [9].

properties of the tunnel contact dominate the current spin polarization. For instance, the spin polarization of electrons injected into GaAs quantum well has been shown to be dominated by the properties of the Fe_3O_4 tunnel contact used [22]. Fe_3O_4 is a ferrimagnetic metal above the Verwey transition temperature (T_V) and a ferrimagnetic insulator below T_V. Hence, the conductivity mismatch is drastically reduced below T_V, increasing the spin polarization (33% at 10K) and injection efficiency as shown in Fig. 3b. As a magnetic insulator, it selectively transmits electrons based on their spin orientation, due to its spin-dependent electronic band structure. Electrons with spins aligned with the magnetic moment of the insulator face a lower energy barrier and can tunnel through more easily, while those with the opposite spin orientation encounter a higher barrier and are less likely to tunnel (Fig. 3a). This results in a highly spin-polarized current emerging from the insulator, as it effectively filters out electrons of the non-preferred spin type. This spin filtering effect can increase the spin injection efficiency into semiconductors.

The Schottky barrier, which forms spontaneously at a FM/SC interface, presents an ideal option for a tunnel barrier. However, for spin-dependent tunneling to occur, the barrier must be reverse-biased. When the device is forward-biased, with a positive voltage applied to the metal relative to the n-type semiconductor (Fig. 4a), the Fermi level of the metal (E_{fm}) drops below that of the semiconductor (E_{fs}). This lowers the barrier height across the semiconductor, allowing electrons to flow from the semiconductor into the metal. In the reverse-biased case, a negative voltage is applied to the metal relative to the n-type semiconductor (Fig. 4b). This causes E_{fm} to rise above E_{fs}, increasing the barrier height $(q\phi_B)$. As a result, the barrier becomes more resistive, impeding the flow of electrons from the metal to the semiconductor. In this configuration, the Schottky barrier acts as an effective tunnel barrier. Notably, Hanbicki *et al.* [23] reported spin injection from a
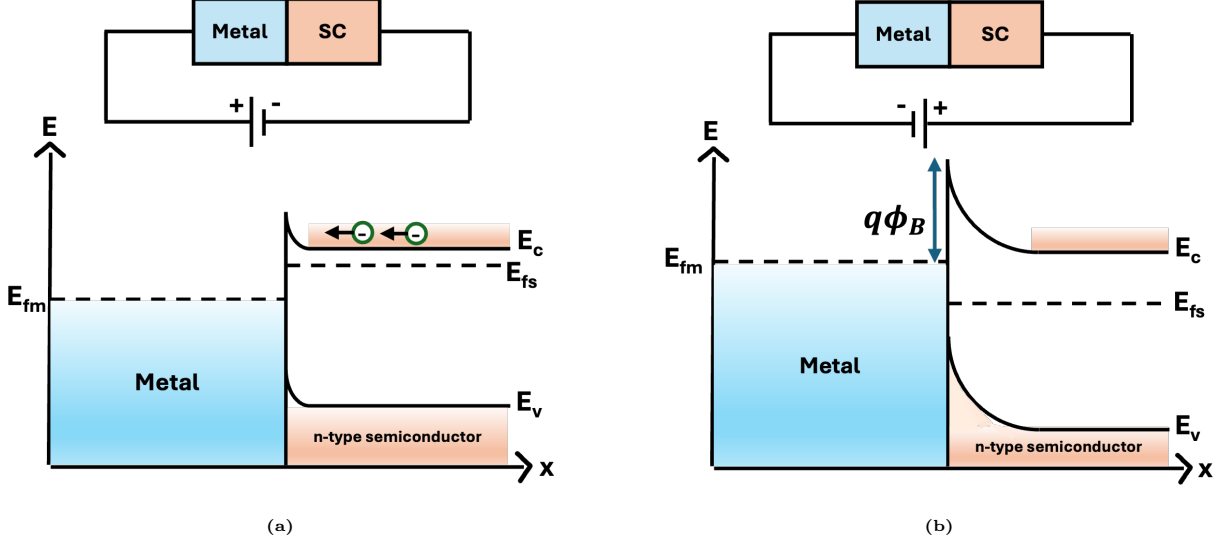
FIG. 4: Energy band diagram of a metal-semiconductor (SC) device under (a) forward bias (b) reverse bias

reverse-biased Fe/AlGaAs Schottky contact into a GaAs quantum well, achieving a 32% net spin polarization at 4.5 K. Recently, a spin injection efficiency of 21% has been achieved in heavily doped n-GaN using the Schottky barrier [24].

Oxide barriers can also address the conductance mismatch issue. The thickness of this barrier significantly influences the spin accumulation in the semiconductor. If the barrier is too thick, the tunneling probability of spin-polarized electrons decreases, thereby reducing spin accumulation. Conversely, if the barrier is too thin, the formation of pinholes occurs, leading to reduced spin accumulation and lower spin injection efficiency. Room-temperature electrical spin injection in both n-type and p-type Si using $Ni_{80}Fe_{20}/Al_2O_3$ contacts were first reported by Dash *et al.* [25]. In heavily doped n-Si, a 142 ps spin lifetime and a spin diffusion length of 230 nm were recorded. Also, in doped p-type Si, a 270 ps spin lifetime and a 310 nm hole spin diffusion length were observed. Other oxide barriers such as MgO [26–28], SiO_2 [29], GaO_x [30] have been used as tunnel barriers to inject spins into semiconductors.

Van der Waal materials are also excellent candidates as tunneling barriers. Monolayer graphene has been used as a tunnel barrier to inject and detect spins in Si at room temperature. The resistance-area (RA) products obtained are three orders of magnitude lower compared to those achieved with oxide barriers on silicon substrates at equivalent doping levels [21]. Recently, Lin *et al.* [31] demonstrated efficient spin injection in n-GaN using an h-BN tunneling barrier at room temperature. By adopting a three-terminal device with Fe, Co, and CoFeB as spin injectors, they showed that CoFeB was a better spin injector compared to the others with a spin relaxation time of 51ps and spin diffusion length of 182nm, which is significantly better than previously reported

results with an Al_2O_3 tunneling barrier [32]. CoFeB was further investigated in a non-local spin valve configuration using both bilayer and monolayer h-BN as tunneling barriers. The study revealed that the spin polarization with bilayer h-BN tunneling barrier was higher compared to that with a monolayer h-BN. This enhancement is attributed to the smoother interface and higher tunneling potential barrier with bilayer h-BN, which effectively mitigates the conductivity mismatch between CoFeB and GaN.

In addition to electrical methods of spin injection, the thermal approach has also been explored. In 2011, Breton $et\ al.$ [33] demonstrated that spin accumulation can be induced in silicon through Seebeck spin tunneling. In their experiment, Si was heated by applying a constant current through Cr/Au contacts positioned at opposite ends of the sample, creating a temperature gradient (ΔT) between Si and the ferromagnetic electrode. This gradient drives electrons with either majority or minority spins from the $Ni_{80}Fe_{20}$ electrode into Si through a SiO_2/Al_2O_3 tunnel barrier, with the induced spin accumulation changing sign when the temperature gradient is reversed. The Hanle effect which describes the depolarization of electron spins due to their precession in a magnetic field can be used to obtain parameters such as spin lifetime and spin accumulation. Hanle measurements (Fig. 5a) revealed that the thermally induced spin accumulation in Si is 0.87 meV. Notably, the Hanle curves were identical for both directions of the current density (J), indicating that the sign and magnitude of the induced spin accumulation remain consistent regardless of the current direction (Fig. 5b).

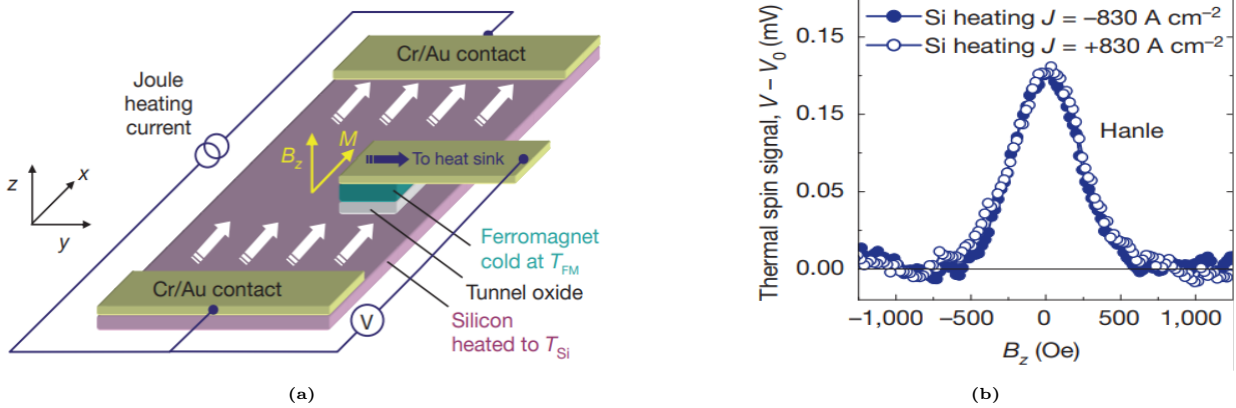(a)   (b)

FIG. 5: (a) Device layout (b) Thermal spin signal as a function of the perpendicular magnetic field, B_z for opposite heating current directions [33].

III. SPIN MANIPULATION AND DETECTION

The spin orientation of injected spin-polarized electrons in the semiconductor may eventually become randomized due to various spin relaxation mechanisms. These include the D'yakonov-Perel mechanism, arising from the spin-splitting of the conduction band due to material inversion asymmetry, leading to the precession of electron spins in random directions [34]; the Elliot-Yafet mechanism arising from spin-orbit coupling during electron scattering processes, where each scattering event can flip the electron's spin [35]; the Bir-Aronov-Pikus mechanism, resulting from the exchange interaction between electrons and holes, causing spin relaxation through recombination process [36]; and hyperfine relaxation, resulting from the interaction between electron spins and nuclear spins, leading to spin dephasing [37].

A. Optical detection

The optical approach to spin detection quantifies the spin polarization of electrons in semiconductors. In this method, spin-polarized electrons in the conduction band recombine with unpolarized holes in the valence band, emitting photons with an optical circular polarization, $\gamma = \frac{1}{2}\frac{n^\uparrow - n^\downarrow}{n^\uparrow + n^\downarrow}$ where $n^\uparrow(n^\downarrow)$ are the number of spin-up (spin-down) electrons recombining with holes. According to optical transition selection rules, assuming the spin quantization axis of the carriers is in the same direction as the emitted photon [8], a spin-up electron can only recombine with either a hole of spin -1/2 or +3/2 as shown in Fig. 6a. Conversely, a spin-down electron can only recombine with either a hole of spin +1/2 or -3/2. This is because the emitted photon carries a spin ± 1, which must be conserved in the recombination process. The spin polarization P_s of the injected electrons is closely related to the circular polarization P_c of the emitted photon by the relation $P_s = 2P_c$. The spin polarization measured using this method is considered a lower bound because various relaxation mechanisms may have caused partial depolarization of the spins before recombination occurs. Successful room temperature spin injection from Fe into GaAs with $\sim 2\%$ spin injection efficiency has been demonstrated through the observation of circular polarization in the electroluminescence of a GaAs/(In, Ga)As LED [38]. Despite silicon being an indirect bandgap semiconductor, successful spin injection from Fe through an Al_2O_3 tunnel barrier into Si (Fig. 6b) was first optically detected by Jonker *et al.* [39] in 2007. The Fe magnetization was mirrored by the circular polarization of the electroluminescence (Fig. 6c), confirming that the source of the injected spin-polarized electrons was the Fe contact. A 30% spin polarization was estimated at 5K.
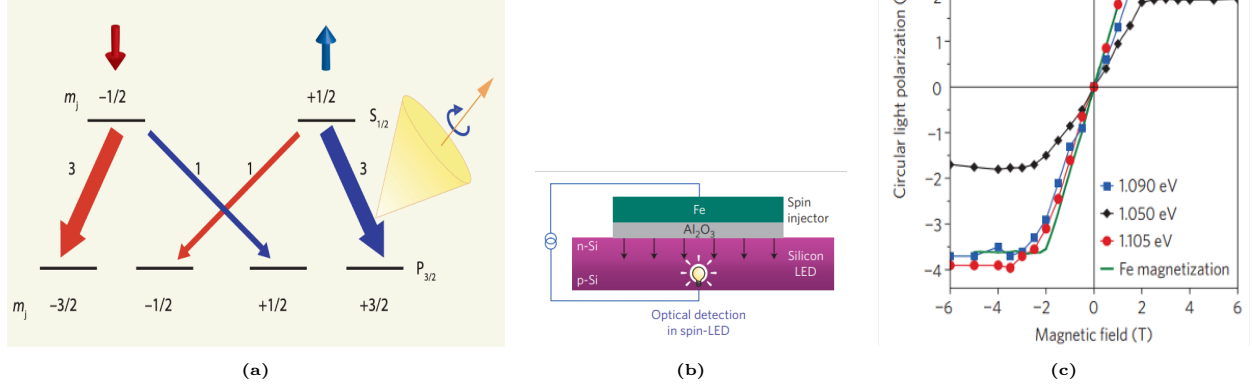
FIG. 6: (a) Polarized light emission governed by optical transition selection rules [9] (b) Schematics of a spin-LED (c) Circular light polarization as a function of magnetic field [39].

B. Electrical detection

Spin accumulation can also be detected electrically because the total tunnel current $I = I^\uparrow + I^\downarrow$ depends on the spin accumulation, $\Delta\mu$ as follows [10]:

$$I = GV - P_G G \left(\frac{\Delta\mu}{2}\right) \tag{7}$$

where P_G is the tunnel spin polarization and G is the total conductance. By rewriting equation 7:

$$V = R_{tun}I + \left(\frac{P_G}{2}\right)\Delta\mu \tag{8}$$

where $R_{tun} = 1/G$.

The two major device configurations for spin injection and detection include the three-terminal (3T) and non-local (NL) geometries. In the three-terminal (3T) configuration (Fig. 7a), spin polarization in the semiconductor is generated and detected using a single ferromagnetic contact. Hence, the spin accumulation measured is directly beneath the ferromagnetic contact where it is largest [10]. When a magnetic field B is applied at an angle θ, the spins precess about the magnetic field. This spin precession causes a decay in $\Delta\mu$. As the magnetic field is increased, the precession frequency $\omega = g\mu_B B/\hbar$ also increases resulting in further decay in the spin accumulation (Fig. 8a). Assuming the R_{tun} is sufficiently large leading to a negligible contribution to $\Delta\mu$ from the ferromagnetic injector, the spin accumulation is given by [10]:

$$\Delta\mu = \Delta\mu(0) \left(cos^2\theta + \frac{sin^2\theta}{1 + (\omega\tau_s)^2} \right) \tag{9}$$

where $\Delta\mu(0)$ is the spin accumulation when $B = 0$, and τ_s is the spin lifetime.
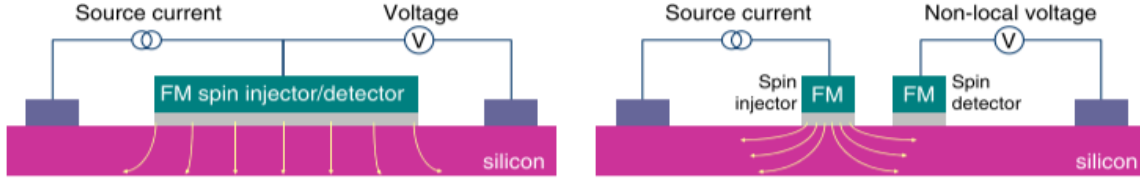

FIG. 7: Electrical injection and detection in the (a) three-terminal (3T) and (b) non-local (NL) geometry [10].

Experimentally, a fixed bias current is applied and the voltage change is measured via a lock-in amplifier when the magnetic field is applied perpendicular to the spins. The voltage change can be obtained from equation 8 as $\Delta V_{Hanle} = \frac{P_G}{2}\Delta\mu(0)$. By plotting ΔV_{Hanle} as a function of B and fitting the Lorentzian in equation 9 when $\theta = 90^o$, the spin lifetime τ_s can be obtained. Furthermore, the spin diffusion length can be calculated based on the relation $\lambda_s = \sqrt{(D\tau_s)}$, where $D = k_B T\mu/q$ is the diffusion constant, T is the absolute temperature, μ is the carrier mobility, k_B is the Boltzmann constant, and q is the charge of electrons.
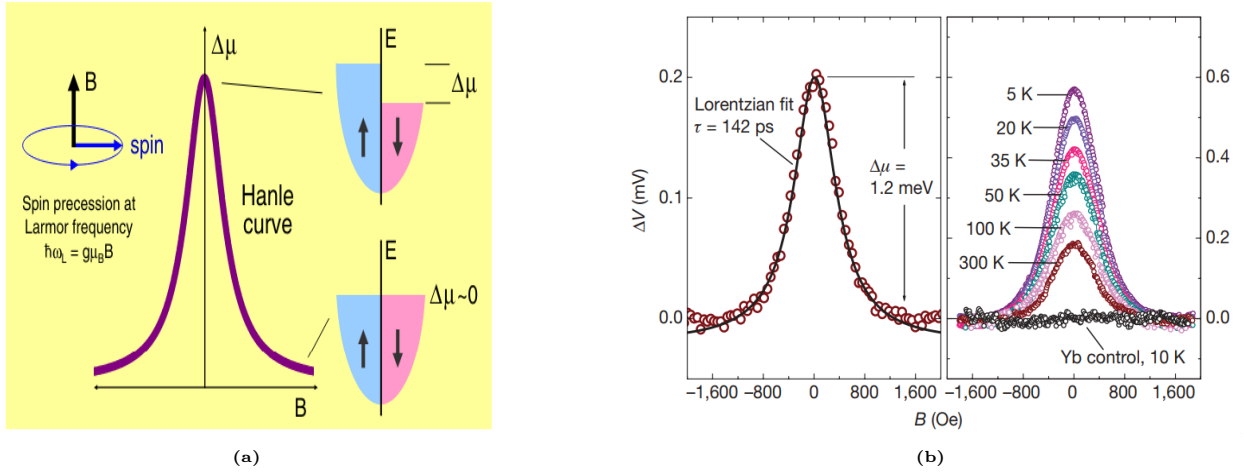

FIG. 8: (a) Schematic of the Hanle effect [10] (b) Hanle curves obtained from a n-Si/Al$_2$O$_3$/Ni$_{80}$Fe$_{20}$/Co tunnel junction at 300 K. Image on the right shows the Hanle curves at various temperatures [25].

The presence of ferromagnetic contacts can introduce spurious signals into the true spin transport signals, caused by local magnetic stray fields, magnetoresistive effects, and alterations in the carrier transport parameters of the semiconductor [10]. To address this, Patel *et al.* [40] demonstrated that

the interface sensitivity of spin-polarized tunneling could be exploited by introducing a nanolayer of a low-work function nonmagnetic material, such as Yb, between the tunnel barrier and the ferromagnetic electrode. By employing this approach, the spin polarization of the tunnel current is suppressed without generating any Schottky barrier, thereby eliminating the true spin signals while retaining any artifacts. This control experiment can effectively determine whether the Hanle signal originates from spin accumulation induced by the injection of spin-polarized tunnel current. In a 3T device comprising of a $Ni_{80}Fe_{20}/Al_2O_3$ tunnel contact on n-Si, Dash $et.$ al [25] reported a large spin accumulation of 1.2 meV and a spin lifetime of 142 ps. Furthermore, by introducing a 2nm layer of Yb between $Ni_{80}Fe_{20}$ and Al_2O_3, the Hanle signal is completely suppressed as shown in Fig. 8b.

In the four-terminal NL geometry (Fig. 7b), a lateral device configuration is used where a spin-polarized current is injected from a ferromagnetic electrode into the semiconductor. The spin current diffuses through the semiconductor without an accompanying charge current, creating a region of spin accumulation. A second ferromagnetic electrode, positioned at a distance from the injection point, detects this spin accumulation by measuring a voltage signal (ΔV_{nl}) induced by the spin-dependent electrochemical potential. The non-local magnetoresistance is expresssed as [24]:

$$\Delta R_{nl} = \frac{\Delta V_{nl}}{I} = \frac{P^2 \rho \lambda_s}{A} exp\left(\frac{-L}{\lambda_s}\right) \tag{10}$$

where ρ is the resistivity of the semiconductor, A is the cross sectional area, λ_s is the spin diffusion length, L is the distance between the spin injector and detector, and P is the spin-injection polarization.

Figure 9 illustrates a non-local lateral spin valve setup with five epitaxial Fe Schottky-tunnel-barrier contacts, each with dimensions of 10 μm x 50 μm, patterned on lightly n-doped GaAs. The central contacts are spaced 12 μm apart, while the two end contacts are set 160 μm from the central trio. Through contact 3, spin-polarized electrons are fed into the GaAs channel and move towards contact 1, while the voltage difference (ΔV) is measured non-locally between contacts 4 and 5. To conduct the spin valve measurement, the magnetic field is varied along the magnetic easy axis while monitoring voltage changes within the field range where the magnetizations of contacts 3 and 4 are aligned antiparallel [41]. The data obtained indicate that the spin polarization of GaAs at 50 K is 2%. Additionally, Hanle measurements were conducted with the magnetizations of contacts 3 and 4 in both parallel and antiparallel configurations (Fig. 9c), revealing a measured spin diffusion length of 6 μm at 50K.

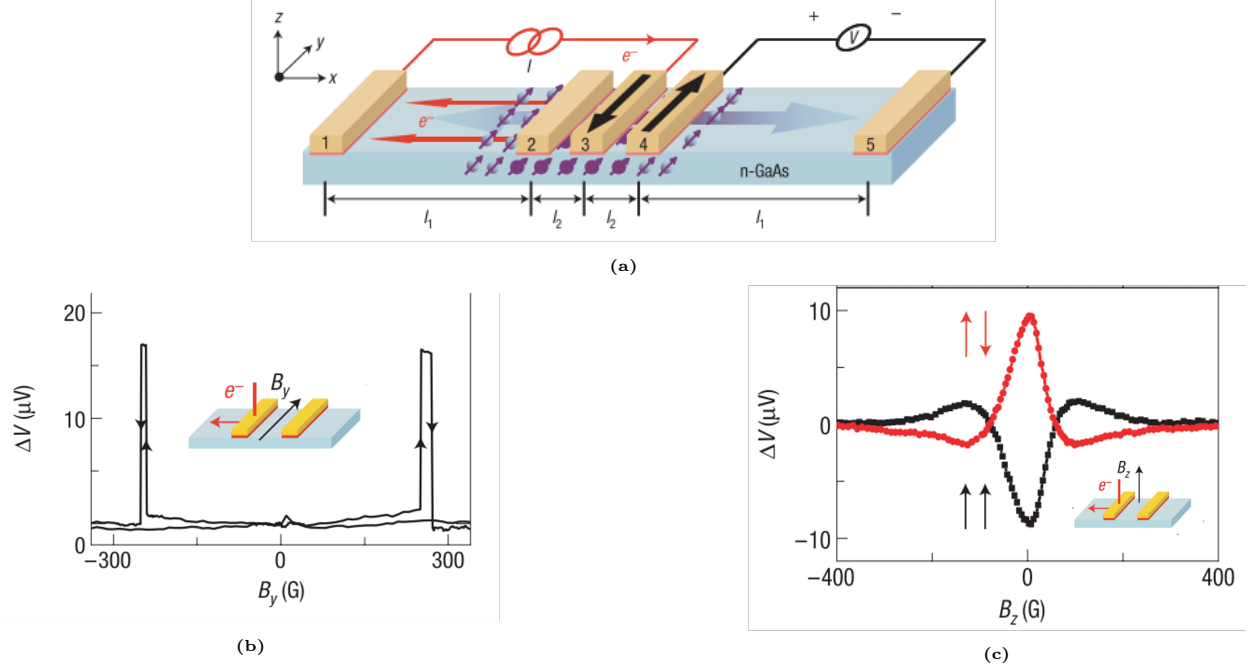FIG. 9: (a) Schematic diagram of the non-local lateral spin valve consisting of five Fe electrodes on n-GaAs. (b) Non-local voltage (ΔV) as a function of B_y, swept in both directions at a current $I_{1,3} = 1.0$ mA at 50 K with the background corrected. Inset shows the direction of the in-plane magnetic field. (c) Non-local voltage versus B_z at the same bias conditions and temperature. The inset shows the dirrection of the perpendicular magnetic field [41].

IV. RECENT DEVELOPMENTS AND CONCLUSION

Chiral-induced spin selectivity (CISS) has recently been explored as a method for generating spin-polarized currents without the need for external magnetic fields or ferromagnetic materials. CISS leverages the intrinsic chirality and spin-orbit coupling of certain materials to selectively filter electron spins, generating spin-polarized currents. This property has been explored in chiral metal-halide perovskite (c-MHP) semiconductors. In 2021, Kim *et al.* [42] used c-MHP semiconductors to demonstrate a spin-LED emitting polarized light with 2.6% degree of circular polarization (DOCP) at room temperature. Hautzinger *et al.* [43] recently demonstrated room-temperature spin injection into $(Al_xGa_{1-x})_{0.5}In_{0.5}P$, a standard III-V semiconductor using chiral semiconductors based on halide perovskites. The measured spin lifetime $\tau_s \approx 100$ ps. By analyzing the emitted circularly polarized light, the DOCP was estimated to be $15 \pm 4\%$. This high spin-injection efficiency can be attributed to the direct semiconductor/semiconductor interface, which heralds a new generation of semiconductor-based spin injectors for various spin functionalities.

In this review, we have examined the key advancements and ongoing challenges in the injection, manipulation, and detection of spin polarization in semiconductors. Although considerable progress has been achieved in both theoretical and experimental fronts, semiconductor spintronics

still encounters significant obstacles that need to be overcome to fully harness its potential. Future efforts should prioritize the development of improved spin injectors with low work function and high spin polarization at room temperature, the exploration of semiconducting 2D materials, and the creation of more efficient detection methods.

[1] G. Lampel, Nuclear dynamic polarization by optical electronic saturation and optical pumping in semiconductors, Phys. Rev. Lett. **20**, 491 (1968).

[2] R. Jansen, Silicon spintronics, Nature Materials **11**, 400 (2012).

[3] S. Datta and B. Das, Electronic analog of the electro-optic modulator, Applied Physics Letters **56**, 665 (1990).

[4] R. Fiederling, M. Keim, G. Reuscher, W. Ossau, G. Schmidt, A. Waag, and L. W. Molenkamp, Injection and detection of a spin-polarized current in a light-emitting diode, Nature **402**, 787 (1999).

[5] B. Behin-Aein, D. Datta, S. Salahuddin, and S. Datta, Proposal for an all-spin logic device with built-in memory, Nature Nanotechnology **5**, 266 (2010).

[6] T. Tanamoto, H. Sugiyama, T. Inokuchi, T. Marukame, M. Ishikawa, K. Ikegami, and Y. Saito, Scalability of spin field programmable gate arrray: A reconfigurable architecture based on spin metal-oxide-semiconductor field effect transistor, Journal of Applied Physics **109**, 10.1063/1.3537923 (2011).

[7] G. Schmidt, D. Ferrand, L. W. Molenkamp, A. T. Filip, and B. J. van Wees, Fundamental obstacle for electrical spin injection from a ferromagnetic metal into a diffusive semiconductor, Phys. Rev. B **62**, R4790 (2000).

[8] G. Schmidt, Concepts for spin injection into semiconductors-a review, Journal of Physics D: Applied Physics **38**, 10.1088/0022-3727/38/7/R01 (2005).

[9] T. Taniyama, E. Wada, M. Itoh, and M. Yamaguchi, Electrical and optical spin injection in ferromagnet/semiconductor heterostructures, NPG Asia Materials **3**, 65 (2011).

[10] R. Jansen, S. P. Dash, S. Sharma, and B. C. Min, Silicon spintronics with ferromagnetic tunnel devices, Semiconductor Science and Technology **27**, 10.1088/0268-1242/27/8/083001 (2012).

[11] Y. Ohno, D. Young, B. Beschoten, F. Matsukura, H. Ohno, and D. Awschalom, Electrical spin injection in a ferromagnetic semiconductor heterostructure, Nature **402**, 790 (1999).

[12] R. Farshchi and M. Ramsteiner, Spin injection from Heusler alloys into semiconductors: A materials perspective, Journal of Applied Physics **113**, 10.1063/1.4802504 (2013).

[13] G. R. Mackay, C. Blaauw, J. Judah, . Al, and S. Asano, Hyperfine fields and electronic structures of the Heusler alloys Co_2MnX (X=Al, Ga, Si, Ge, Sn), J. Phys.: Condens. Matter **2**, 8583 (1990).

[14] I. Galanakis, P. H. Dederichs, and N. Papanikolaou, Slater-Pauling behavior and origin of the half-metallicity of the full-Heusler alloys, Physical Review B - Condensed Matter and Materials Physics **66**, 1 (2002).

[15] W. H. Wang, M. Przybylski, W. Kuch, L. I. Chelaru, J. Wang, Y. F. Lu, J. Barthel, H. L. Meyerheim, and J. Kirschner, Magnetic properties and spin polarization of Co_2MnSi Heusler alloy thin films epitaxially grown on GaAs(001), Physical Review B - Condensed Matter and Materials Physics **71**, 10.1103/PhysRevB.71.144416 (2005).

[16] M. Ramsteiner, O. Brandt, T. Flissikowski, H. T. Grahn, M. Hashimoto, J. Herfort, and H. Kostial, Co_2FeSi/GaAs/(Al,Ga)As spin light-emitting diodes: Competition between spin injection and ultrafast spin alignment, Physical Review B - Condensed Matter and Materials Physics **78**, 10.1103/PhysRevB.78.121303 (2008).

[17] M. Hashimoto, J. Herfort, A. Trampert, H. P. Schönherr, and K. H. Ploog, Growth temperature dependent interfacial reaction of Heusler-alloy Co_2FeSi/GaAs(001) hybrid structures, Journal of Physics D: Applied Physics **40**, 1631 (2007).

[18] X. Y. Dong, C. Adelmann, J. Q. Xie, C. J. Palmstrøm, X. Lou, J. Strand, P. A. Crowell, J. P. Barnes, and A. K. Petford-Long, Spin injection from the Heusler alloy Co_2MnGe into $Al_{0.1}Ga_{0.9}As$GaAs heterostructures, Applied Physics Letters **86**, 1 (2005).

[19] C. D. Damsgaard, M. C. Hickey, S. N. Holmes, R. Feidenhans'L, S. O. Mariager, C. S. Jacobsen, and J. B. Hansen, Interfacial, electrical, and spin-injection properties of epitaxial Co_2MnGa grown on GaAs(100), Journal of Applied Physics **105**, 10.1063/1.3148298 (2009).

[20] E. I. Rashba, Theory of electrical spin injection: Tunnel contacts as a solution of the conductivity mismatch problem, Phys. Rev. B **62**, R16267 (2000).

[21] O. M. V. Erve, A. L. Friedman, E. Cobas, C. H. Li, J. T. Robinson, and B. T. Jonker, Low-resistance spin injection into silicon using graphene tunnel barriers, Nature Nanotechnology **7**, 737 (2012).

[22] E. Wada, K. Watanabe, Y. Shirahata, M. Itoh, M. Yamaguchi, and T. Taniyama, Efficient spin injection into GaAs quantum well across Fe_3O_4 spin filter, Applied Physics Letters **96**, 10.1063/1.3357436 (2010).

[23] A. T. Hanbicki, O. M. V. Erve, R. Magno, G. Kioseoglou, C. H. Li, B. T. Jonker, G. Itskos, R. Mallory, M. Yasar, and A. Petrou, Analysis of the transport process providing spin injection through an Fe/AlGaAs Schottky barrier, Applied Physics Letters **82**, 4092 (2003).

[24] Z. Sun, N. Tang, S. Zhang, S. Chen, X. Liu, and B. Shen, Spin injection, relaxation, and manipulation in GaN-based semiconductors, Advances in Physics: X **8**, 10.1080/23746149.2022.2158757 (2023).

[25] S. P. Dash, S. Sharma, R. S. Patel, M. P. D. Jong, and R. Jansen, Electrical creation of spin polarization in silicon at room temperature, Nature **462**, 491 (2009).

[26] G. Salis, R. Wang, X. Jiang, R. M. Shelby, S. S. Parkin, S. R. Bank, and J. S. Harris, Temperature independence of the spin-injection efficiency of a MgO-based tunnel spin injector, Applied Physics Letters **87**, 1 (2005).

[27] H. Kum, J. Heo, S. Jahangir, A. Banerjee, W. Guo, and P. Bhattacharya, Room temperature single GaN nanowire spin valves with FeCo/MgO tunnel contacts, Applied Physics Letters **100**, 10.1063/1.4711850 (2012).

[28] S. G. Bhat and P. S. Kumar, Room temperature electrical spin injection into GaAs by an oxide spin

injector, Scientific Reports **4**, 10.1038/srep05588 (2014).

[29] C. H. Li, G. Kioseoglou, O. M. V. T. Erve, P. E. Thompson, and B. T. Jonker, Electrical spin injection into Si(001) through a SiO_2 tunnel barrier, Applied Physics Letters **95**, 10.1063/1.3254228 (2009).

[30] H. Saito, J. C. L. Breton, V. Zayets, S. Yuasa, and K. Ando, Highly Enhanced Electron-Injection Efficiency in GaAs-Based Light-Emitting Diodes Using a Fe/GaO_x Tunnel Injector, Applied Physics Express **2**, 083003 (2009).

[31] D. Lin, W. Kang, Q. Wu, A. Song, X. Wu, G. Liu, J. Wu, Y. Wu, X. Li, Z. Wu, D. Cai, J. Yin, and J. Kang, High-Efficient Spin Injection in GaN at Room Temperature Through A Van der Waals Tunnelling Barrier, Nanoscale Research Letters **17**, 10.1186/s11671-022-03712-5 (2022).

[32] A. Song, J. Chen, J. Lan, D. Fu, J. Zhou, Z. Zhong, J. Guo, X. Wu, Y. Wu, X. Li, S. Huang, Z. Wu, and J. Kang, Modulating room temperature spin injection into GaN towards the high-efficiency spin-light emitting diodes, Applied Physics Express **13**, 10.35848/1882-0786/ab810b (2020).

[33] J. C. L. Breton, S. Sharma, H. Saito, S. Yuasa, and R. Jansen, Thermal spin current from a ferromagnet to silicon by Seebeck spin tunnelling, Nature **475**, 82 (2011).

[34] M. I. Dyakonov and V. I. Perel, Current-induced spin orientation of electrons in semiconductors, Physics Letters A **35**, 459 (1971).

[35] R. J. Elliott, Theory of the Effect of Spin-Orbit Coupling on Magnetic Resonance in Some Semiconductors, Phys. Rev. **96**, 266 (1954).

[36] G. L. Bir, A. G. Aronov, and G. E. Pikus, Spin relaxation of electrons due to scattering by holes, Zh. Eksp. Toer. Fiz. **69**, 1382 (1975).

[37] M. I. D'yakonov and V. I. Perel', Optical orientation in a system of electrons and lattice nuclei in semiconductors. Theory, Zh. Eksp. Toer. Fiz. **65**, 362 (1973).

[38] H. J. Zhu, M. Ramsteiner, H. Kostial, M. Wassermeier, H. P. Schönherr, and K. H. Ploog, Room-temperature spin injection from Fe into GaAs, Physical Review Letters **87**, 10.1103/PhysRevLett.87.016601 (2001).

[39] B. T. Jonker, G. Kioseoglou, A. T. Hanbicki, C. H. Li, and P. E. Thompson, Electrical spin-injection into silicon from a ferromagnetic metal/tunnel barrier contact, Nature Physics **3**, 542 (2007).

[40] R. S. Patel, S. P. Dash, M. P. D. Jong, and R. Jansen, Magnetic tunnel contacts to silicon with low-work-function ytterbium nanolayers, Journal of Applied Physics **106**, 10.1063/1.3159638 (2009).

[41] X. Lou, C. Adelmann, S. A. Crooker, E. S. Garlid, J. Zhang, K. S. Reddy, S. D. Flexner, C. J. Palmstrøm, and P. A. Crowell, Electrical detection of spin transport in lateral ferromagnet-semiconductor devices, Nature Physics **3**, 197 (2007).

[42] Y.-H. Kim, Y. Zhai, H. Lu, X. Pan, C. Xiao, E. A. Gaulding, S. P. Harvey, J. J. Berry, Z. V. Vardeny, J. M. Luther, and M. C. Beard, Chiral-induced spin selectivity enables a room-temperature spin light-emitting diode, Science **371**, 2024 (2021).

[43] M. P. Hautzinger, X. Pan, S. C. Hayden, J. Y. Ye, Q. Jiang, M. J. Wilson, A. J. Phillips, Y. Dong, E. K. Raulerson, I. A. Leahy, C.-S. Jiang, J. L. Blackburn, J. M. Luther, Y. Lu, K. Jungjohann, Z. V.

Vardeny, J. J. Berry, K. Alberi, and M. C. Beard, Room-temperature spin injection across a chiral perovskite/III–V interface, Nature 10.1038/s41586-024-07560-4 (2024).